



## ORIGINAL ARTICLE

# Longitudinal shear strength design of composite slabs by full-scale FE modelling considering the embossments

*Resistência ao cisalhamento longitudinal de lajes mistas modeladas em escala real considerando a geometria das moças por meio do método dos elementos finitos*

Juçara Hingrid Lima Pinheiro Mello<sup>a</sup>

Dennis Quaresma Pureza<sup>a</sup>

Maurício Prado Martins<sup>a</sup>

Hermano de Sousa Cardoso<sup>b</sup>

Rodrigo de Melo Lameiras<sup>a</sup>

Luis Augusto Conte Mendes Veloso<sup>a</sup>

José Luís Vital de Brito<sup>a</sup>

José Guilherme Santos da Silva<sup>c</sup>

Guilherme Santana Alencar<sup>a</sup>

<sup>a</sup>Universidade de Brasília – UnB, Faculdade de Tecnologia – FT, Programa de Pós-graduação em Estruturas e Construção Civil – PECC, Brasília, DF, Brasil

<sup>b</sup>Global R&D Brazil, ArcelorMittal, Serra, ES, Brasil

<sup>c</sup>Universidade do Estado do Rio de Janeiro – UERJ, Faculdade de Engenharia – FEN, Programa de Pós-graduação em Engenharia Civil – PGECIV, Rio de Janeiro, RJ, Brasil

Received 02 June 2023

Accepted 11 October 2023

**Abstract:** Slabs with cast-in-place steel formwork are composite structural elements composed of concrete and steel. The horizontal shear failure mode is the most common in composite slabs based on numerous experimental studies. This failure mode consists of loss of adherence and mechanical contact at the interface of the composite system and often occurs before the system reaches its full bending capacity. Thus, the design of this constructive system is determined by the value of the longitudinal shear strength, which can be computed by the semi-empirical so-called traditional  $m-k$  method based on the four-point bending test proposed by several standards. One of the most known factors to influence the longitudinal shear strength is the geometry of embossments present in the steel work. Calibrated computational simulation using the finite element method can be an alternative way to simulate this type of test. The present work modified and adapted a methodology explicitly including the geometry of embossments in the analysis in order to use materials and products with characteristics available to structural engineers in Brazil and used this methodology to derive  $m-k$  coefficients. This is being made with the objective of numerically simulating the effect of relevant parameters for determining the longitudinal shear strength at the concrete-steel interface of composite slabs. Force versus slip, force versus displacement graphs were obtained and the  $m-k$  coefficient values found were compared with those of other authors in the literature. The simulations presented values consistent with the literature and in relation to the rupture mode by longitudinal shear, the numerical simulations performed presented ultimate strengths with goodness-of-fit measured by the conventional coefficient of determination, reaching a good value for the semi-empirical relation using the results of the finite element data.

**Keywords:** composite slabs, steel deck, longitudinal shear, numerical analyses, finite element modelling.

**Resumo:** Lajes com fôrmas metálicas utilizadas durante a concretagem são um sistema estrutural misto composto de aço e concreto. O modo de falha por cisalhamento horizontal é o mais comum em lajes mistas com bases em numerosos estudos experimentais. Esta falha consiste na perda de aderência e contato mecânico do sistema misto e, frequentemente, ocorre antes do sistema atingir sua capacidade máxima à flexão plástica.

**Corresponding author:** Juçara Hingrid Lima Pinheiro Mello. E-mail: [j.hingrid2@gmail.com](mailto:j.hingrid2@gmail.com)

**Financial support:** Coordenação de Aperfeiçoamento de Pessoal de Nível Superior (CAPES). Scholarship nº: 88887.638209/2021-00.

**Conflict of interest:** Nothing to declare.

**Data Availability:** the data that support the findings of this study are available from the corresponding author, Juçara H. Lima Pinheiro Mello, upon reasonable request.



This is an Open Access article distributed under the terms of the Creative Commons Attribution License, which permits unrestricted use, distribution, and reproduction in any medium, provided the original work is properly cited.

Assim, o projeto deste sistema construtivo é determinado pela sua resistência ao cisalhamento longitudinal, que pode ser determinada pelo método semiempírico convencional  $m-k$  com base no ensaio de flexão de quatro pontos proposto por diversas normas. Um dos fatores conhecidos de maior influência na resistência ao cisalhamento longitudinal é a geometria das mossas presentes na fôrma metálica. Simulações computacionais por meio do método dos elementos finitos calibradas com base em resultados experimentais podem ser uma alternativa à realização deste tipo de ensaio. O presente trabalho modificou e adaptou uma metodologia que inclui explicitamente a geometria das mossas na análise de modo a usar materiais e produtos com características disponíveis para os engenheiros estruturais do Brasil e usou esta metodologia para derivar coeficientes  $m-k$ . Isto foi feito com o objetivo de simular numericamente o efeito de parâmetros relevantes para determinar a resistência ao cisalhamento longitudinal na interface aço-concreto de lajes mistas. Gráficos de força versus deslocamentos foram obtidos e os valores dos coeficientes  $m-k$  foram comparados com aqueles de outros autores na literatura. As simulações apresentaram valores consistentes com a literatura e, em relação ao modo de ruptura por cisalhamento longitudinal, as simulações numéricas realizadas apresentaram resistências últimas com bom ajuste medido pelo coeficiente de determinação convencional chegando a um valor bom para a relação semiempírica utilizando os resultados dos dados de elementos finitos.

**Palavras-chave:** lajes mistas, steel deck, cisalhamento longitudinal, análises numéricas, modelagem em elementos finitos.

---

**How to cite:** J. H. L. P. Mello et al. "Longitudinal shear strength design of composite slabs by full-scale FE modelling considering the embossments," *Rev. IBRACON Estrut. Mater.*, vol. 17, no. 5, e17505, 2024, <https://doi.org/10.1590/S1983-41952024000500005>

## 1 INTRODUCTION

The use of composite structures in civil construction arose from the need to protect the building from fire damage. At first it was not the objective to make the use of steel with reinforced concrete a structural element; however, by verifying the use of these materials together, it was possible to find an efficient, economical and sustainable construction method for this purpose. The steel deck slab is a composite structural element by concrete and steel. In the final phase of its construction process, the concrete acts structurally together with the steel deck, and the latter can partially or completely replace the slab's tensile reinforcement. In the initial phase, before the concrete reaches 75% of the specified compressive strength, the steel deck, supports the permanent actions and the construction overload alone, as presented in ABNT NBR 8800 [1].

The composite behavior of the slab depends on its ability to resist the shear forces present at the steel-concrete interface. Basically, three mechanisms are responsible for the resistant capacity of this interface, they are: the initial adhesion of chemical nature, the mechanical connection (offered by the embossments) and friction. In addition, other variables influence the mechanical behavior presented by composite slabs, the strength of the reinforced concrete cover and the length of the shear span [2].

The verification of this type of slab by the Limit State Method considers the possible failure modes associated to the conditions in which the design loads such as bending moment, longitudinal shear, vertical shear or punching exceed the corresponding design strengths of the slabs. However, failure by longitudinal shear is the most frequent failure mode in composite slabs. This failure mode consists of loss of adhesion and mechanical contact at the interface of the composite system and occurs before the system reaches its full flexural capacity. The design recommended by the existing normative models proposes the use of two calculation methods, namely the  $m-k$  coefficient method and the partial interaction method. To obtain the design resistances from these methods, it is necessary to perform experimental four-point bending tests. This test is described in EN 1994-1-1 [3], and is usually performed by the steel deck manufactures to obtain the  $m-k$  coefficients.

The composite slab with steel deck history started in 1938 when the H.H. Robertson Company used the form work which was known as "keystone beam". The keystone beam was a cellular floor system used primarily in low rise buildings. The steel deck form work was not considered or designed to act compositely with the floor system. The transfer of the horizontal shear between concrete and deck came about when the Granco Steel Products Company combined the deck with wires welded transverse to the ribs. With this it was possible to provide composite action between steel and concrete. "Cofar" was the name of the product, and it gained acceptance and significantly reduced the cost of concrete floor systems at the time [4]. The embossments and indentations within the deck were used in the late 1950's and early 1960's to replace the welded wires used as horizontal shear transfer devices. To meet this charge, several manufactures introduced their version of steel deck. No design standards existed; therefore, individual manufacturers needed to verify that their designs were adequate on their own. This was often done by performing numerous laboratory tests. The American Iron and Steel Institute, in 1967, initiated an extensive research project at Iowa State University (ISU). The objective of this research was to analyse the behavioural characteristics and develop a design standard for composite steel deck reinforce concrete (SDRC) floor systems. With similar objectives, the West Virginia University developed independent studies, in accordance with [5].

In the course of time, it was observed that performing these tests was costly assuming the need for variation of parameters and, consequently, the diversity of prototypes to obtain a satisfactory result. That way, the use of numerical analysis, based on experimental results, after calibrated and validated, could be an alternative to performing more tests [6]. It was possible to verify that with the passing of time and with computational advances some researchers had dedicated themselves to calibrate numerical models in several programs to make the finite element method a viable alternative to execution of more tests.

In this manner, Daniels and Crisnef [7] in 1993 reported in their paper the use of the finite element method in a pioneering way to conduct studies on composite slabs. In this work, a beam element was used, where the connections between steel and concrete were determined through embossments and end anchorage that were defined using approximations of experimental test load-slip data. This was a limitation of the work, besides the fact that it does not present the actual representation of the embossments, mostly due to limited hardware computer of the time.

Following, Shobaki [6] in 2000 modeled composite slab in full scale and small scale, however in the full scale model the author didn't modelled the embossments geometry also due to computational limitations, modelling the longitudinal shear strength indirectly by calibrating a friction coefficient with the software ANSYS. In the small-scale model, it was modelled the geometry of only one embossment, however with simple loading (not the loading derived from a four-point bending test).

Chen and Shi [8] in 2011 used the ANSYS element TARGET173 and element CONTACT170. Similarly to Shobaki [6], the modelling of the embossments geometry was also ignored. The effect of the embossments was also simulated indirectly through contact and friction purely of the plane surfaces, and experimental data from pull-out tests and bending tests were used to validate and calibrate the proposed FE models.

Gholamhoseini et al. [9] in 2014 used Atena 3D software and modelled in full-scale with one rib. In this work the embossments were also not represented. To represent the steel deck-concrete slab contact an interface material based on Mohr-Coulomb criterion with tension cut off was used. The constitutive relation for a general two-dimensional case was given in terms of tractions on the interface planes and relative sliding and opening displacements.

Silva and Silva [10] in 2019 developed full-scale prototypes where it was used the discretization of a composite slab in flat shell elements, beam elements and interface elements. Two interface elements were used to model the steel-concrete interface, one that connects two flat shell elements and the other that connects beam element to the shell element. A linear curve representing total connection, that is, high stiffness was used to represent the contact in the transverse and vertical direction.

Santos and Malite [2] in 2019 developed a numerical simulation with finite elements method through the ABAQUS software. The model was realized in full-scale with a Brazilian formwork, but embossments were not represented. For contact between the formwork and the concrete, a coefficient of friction calibrated with experimental data was used. Gholamhoseini [11] in 2018 carried out a finite element analysis of a continuous composite slab with steel decking, but without explicitly considering embossments geometry.

Soltanalipour et al. [12] in 2022 modelled full-scale models explicitly including embossments via the ANSYS software, with steel sheeting available in Spanish construction sector, made of European steel standard S320. Besides explicitly modelling the embossments geometry, contact elements and a friction coefficient were also used to simulate the contact between both materials. The authors performed a calibration of the models through experimental tests. The main purpose of the work was to study the structural behaviour differences between open-rib versus re-entrant composite slabs, not making inference regarding ultimate shear strength related to the  $m-k$  method.

After this bibliographical survey, it was possible to define the objective of this work as proposes the study of the failure mode by longitudinal shear in composite slabs by performing numerical analysis based on the Finite Element Method (FEM) with the consideration of the physical and geometric nonlinear behavior of the materials. In this context, this work proposes to combine and adapt a methodology developed at the Polytechnic University of Catalonia [12] to perform finite element simulations of four-point bending tests of composite slabs with steel deck, with explicit modeling of the geometry of the embossment, but modifying the embossments geometry to fit to a steel sheeting available in Brazilian construction sector, made of Brazilian steel standard ZAR280. For this purpose, the real dimensions of the steel sheeting were measured *in situ*, as will be illustrated in the next sections. Once the numerical methodology is consolidated for this specific slab, estimates of the ultimate longitudinal shear strength can be reasonable made to obtain  $m-k$  coefficients, also allowing future parametric studies to enlarge the comprehension of the relevant parameters affecting the longitudinal shear failure mode of composite slabs.

### 1.1 Design of composite slabs in longitudinal shear using the m-k method

The m-k method is a semi-empirical method presented by ABNT NBR 8800 [1] and EN1994-1-1 [3] to verify the longitudinal shear strength of composite slabs. That is, to verify the longitudinal shear strength it is used the vertical shear loading. According to these recommendations, the failure mode to longitudinal shear is verified if the maximum design shear force,  $V_{Sd}$ , is lower than the design shear strength of the slabs,  $V_{\ell,Rd}$ , which can be calculated as follows:

$$V_{Sd} \leq V_{\ell,Rd} = \frac{bd_F \left[ \left( \frac{mA_{F,ef}}{bL_s} \right) + k \right]}{\gamma_{s\ell}} \tag{1}$$

Where

$V_{Sd}$  design shear force;

$V_{\ell,Rd}$  design shear strength (failure mode: longitudinal shear);

$d_F$  is the distance from the top of the concrete slab to the geometric center of effective formwork section;

$b$  is the unit width of the slab;

$L_s$  is the shear span;

$m$  and  $k$  are empirical constants (with units of force per area), obtained through test performed according to EN1994-1-1 [3];

$\gamma_{s\ell}$  is the strength weighting coefficient, suggested by EN1994-1-1 [3], equal to 1,25;

$A_{F,ef}$  is the effective cross-sectional area of the steel deck.

The  $m$ - $k$  coefficients are obtained by simple linear regression of the four-point bending test results, in the form  $Y = m \cdot X + k$ , whereby  $Y = V_{l,u} / (b \cdot d_F)$  e  $X = A_{F,ef} / (b \cdot L_s)$ . Where  $V_{l,u}$  is the obtained value of the ultimate shear force considering the self-weight of the slabs.

### 1.2 Four-point bending test

The test method proposed by EN 1994-1-1 [3] consists of applying two lines of loads to a composite slab, which is conventional four-point bending test, as can be seen in Figure 1.

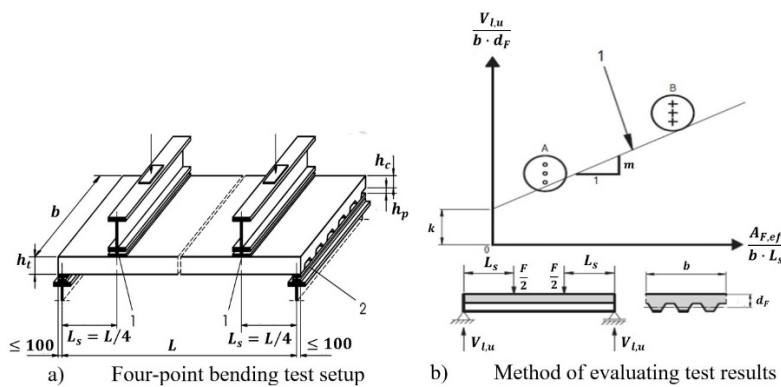


**Figure 1.** Bending test model and graph format to obtain  $m$  and  $k$  coefficients [3].

It is recommended that the test be performed on simply supported slabs, with the test system equal or equivalent to Figure 1. Two equal linear concentrated loads are applied with symmetrical arrangement at  $L/4$  and  $3L/4$  in the span direction. When the tests are used to determine  $m$  and  $k$  coefficients, for each variable to be analysed two groups of three tests (indicated in Figure 1 by zones A and B) or three groups of two tests should be performed. Regarding Figure 1b, for the prototypes in Zone A, the shear span should be as large as possible, but still causing failure by longitudinal shear, and for the prototypes in Zone B, the shear span should be as small as possible, but still causing failure by longitudinal shear, but without having a length less than  $3h_i$ ,  $h_i$  is total height of the slab (Figure 1a). European standard rules the use of crack inducers below the line loads inside the concrete, in order to clearly define the shear span during test. This results in the readily creation of two cracked sections since the beginning of the application of loading during test, disregarding the tensile strength of the concrete in these sections.

## 2 FINITE ELEMENT MODELLING FEATURES AND STRATEGIES

This work was developed using the methodology of numerical-computational simulation based on the finite element program ANSYS, version 2021R2, together with the programming language APDL (ANSYS Programming Design Language). It was used as a basis the methodology presented in the article by Soltanalipour et al. [12] with adaptation for the materials of the construction market in Brazil, in order to include the geometry of a steel deck present in the Brazilian market (see Figure 2), considering the national regulations with the use of the provisions of the standards [1], [13], [14] and [15].

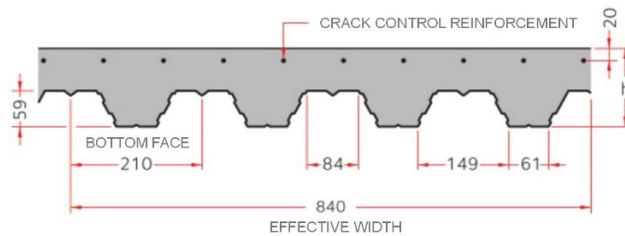


Figure 2. Geometric characteristics of the Polydeck 59s (units in millimetres) [16].

### 2.1 Steel deck material characterization and FE modelling

Experimental characterization of the material was made taking test samples from the lower flange of the steel deck slabs avoiding the longitudinal stiffener region. The geometry of the samples was defined by the ASTM E8/E8M – 13a [17] standard specifications and is shown in Figure 3.

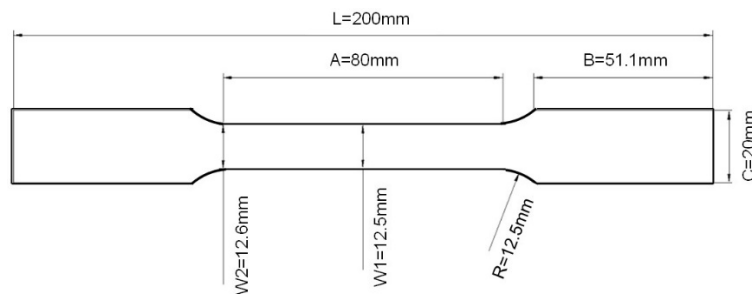


Figure 3. Geometric characteristics of the test samples as per ASTM E8/E8M – 13a [17].

The experimental setup involved an MTS universal testing machine and a *Xsight* commercial 2D digital image correlation (DIC) system. Digital image correlation analysis requires that the surface of the test samples have a random speckled pattern to provide distinguishable features or markers that can be easily tracked. Once the material used did not offered a natural pattern, it was necessary to create an artificial one. The process of fabricating the test samples pattern started with the utilization of fine grain sandpaper in order to optimize material surface adherence. A layer of matte white spray paint primer was applied, and matte black paint speckles were created to achieve a visually distinctive pattern on the surface of the samples, see Figure 4.

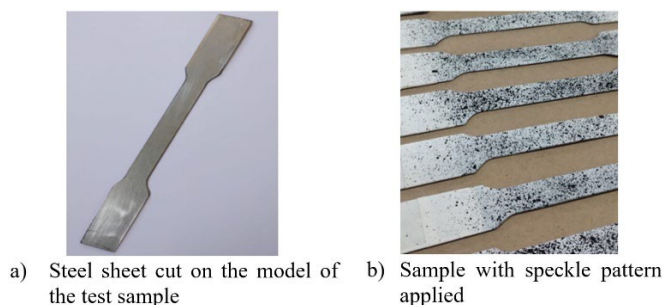
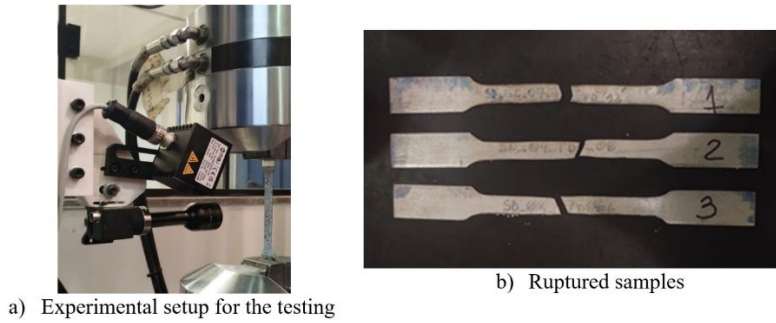


Figure 4. Test Sample.

Three samples were tested in an MTS universal testing machine equipped with the DIC camera and led lighting, see Figure 5a. The ruptured samples are shown in Figure 5b.



**Figure 5.** Test model and tested samples.

A typical stress-strain engineering curve of the tensile strength tests is shown in Figure 6. The yield stress of the tested samples stayed above the nominal value of 280 MPa, reaching a value of about 320 MPa, with a short plastic plateau and then a hardening pattern, typical of steels used for cold formed sections. Therefore, since the aim of the present work is to use finite element method to carry out a lower bound estimation of the longitudinal shear design strength, the value of 280 MPa with an elastic-perfectly plastic curve were used in the present simulations.

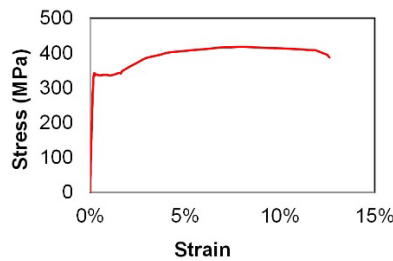


**Figure 6.** Typical stress-strain curve result of the tensile strength test of the ZAR280.

Thus, the constitutive model for the profiled sheet steel adopted is bilinear isotropic, initially as linear elastic, and then as perfectly plastic, that is, a perfect elastoplastic model, both in tension and in compression. The parameters of the steel formwork are given in Table 1.

**Table 1.** Steel deck material parameters.

Constitutive model	Bilinear isotropic
Young's model of steel	200 GPa
Poisson coefficient	0.3
Nominal yield strength	280 MPa
Density	7850 kg/m <sup>3</sup>
Plasticity criterion	von Mises
Tensile strength	Undefined

The steel deck finite element adopted in the modeling was SHELL281 [18] (see Figure 7), which is a finite element with quadratic shape function with 6 degrees of freedom per node (translations and rotations in the three Cartesian directions) and is quite appropriate for very thin sheets that suffer large rotations and deformations in a non-linear regime, which is the case of the steel deck at the end of the four-point bending test. For the region of the embossments, which has a complex geometry, its triangular shape with 6 nodes was used, while for the region away from the embossment, its simpler rectangular shape with 8 nodes is used. This element has, by default, three integration points for each layer and employs full integration scheme. However, when a single layer is defined and plasticity is present, the number of integrations points is changed to a minimum of five during solution [18].

The thickness of the finite elements is the same as the effective thickness of the steel deck, discounting the galvanized coating. For example, Polydeck 59s is commercially available in nominal thicknesses of 0.80, 0.95, and 1.25 millimetres. However, the effective thickness for structural purposes must discount the galvanized coating, which for ZAR 280 with Z275 coating, is of the order of 0.02 millimetres per face. Therefore, the effective thicknesses to be used for these elements will be 0.76, 0.91, and 1.21 millimetres.

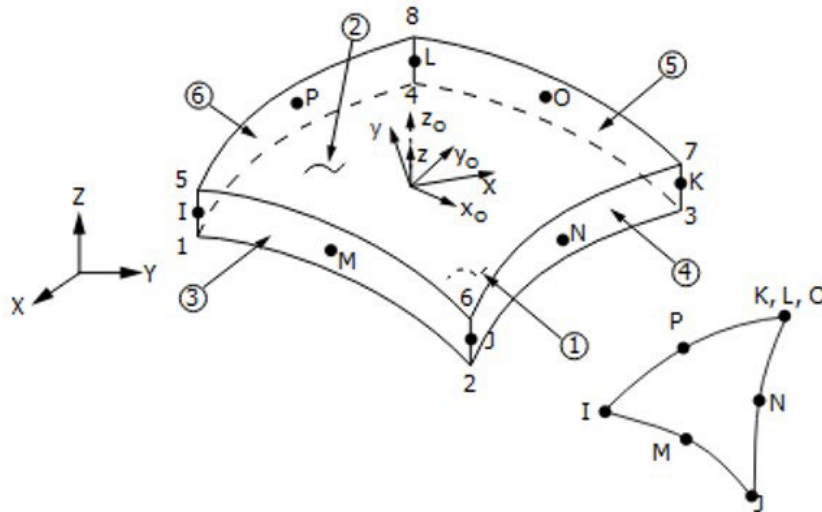


Figure 7. Quadratic shell finite element SHELL281 [18].

## 2.2 Concrete

The constitutive model adopted for the nonlinear behavior of concrete was the Menétrey-Willam model [19], which is based on the plasticity theory and the rupture surface of William and Warnke [20], and was only recently included in recent versions of ANSYS software (since 2021). This model is able to represent many important mechanical behaviours of concrete, for example: tensile strength different from compressive strength, nonlinear hardening, softening and dilatancy angle. The parameters needed in ANSYS to define the concrete failure surface of Menétrey-Willam were the average uniaxial compressive strength ( $f_{cm}$ ), uniaxial tensile strength ( $f_t$ ), biaxial compressive strength ( $f_{bc}$ ) and the dilatancy angle ( $\psi$ ). The softening functions that apply after the compression and tensile limits have been reached were disregarded to avoid convergence difficulties in the nonlinear analysis [12]. The parameters used to represent concrete are shown in Table 2. In order to use a concrete with characteristics of aggregates near the site of Distrito Federal, a concrete material characterization test data from a previous work carried out at University of Brasilia, with  $f_{cm}$  of 41 MPa was used [21].

Table 2. Concrete material parameters.

Constitutive model	Menétrey-Willam
Young's model of concrete	33.6 GPa
Poisson coefficient	0.2
Average compressive strength ( $f_{cm}$ )	41 MPa
Density	2400 kg/m <sup>3</sup>
Ultimate tensile strength uniaxial ( $f_t$ )	$f_{ct,m} = 0.3 f_{ck}^{2/3}$
Biaxial compressive strength ( $f_{bc}$ )	1.2 $f_{cm}$
Dilatancy angle ( $\psi$ )	Thirteen degrees
Softening functions	Disregarded

The finite element adopted for the concrete was the quadratic solid finite element SOLID187 (see Figure 8), with 10 nodes and three degrees of freedom per node (translation in the three Cartesian directions), suitable for modeling and discretization of very irregular geometries. The use of this finite element is necessary due to the complex interface geometry between the steel deck and the concrete volume in the embossments region.

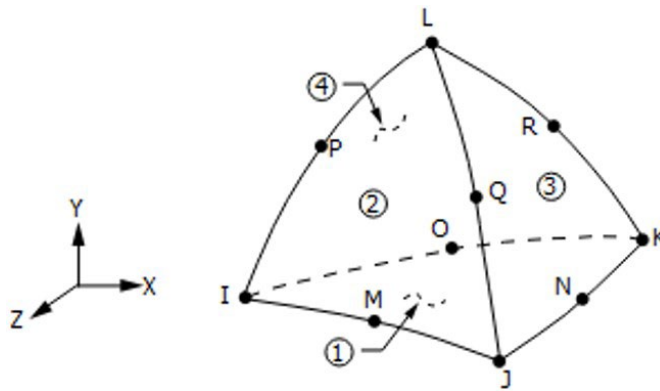


Figure 8. Quadratic solid finite element SOLID187 [18].

### 2.3 Contact between steel deck and concrete

The contact between concrete and steel deck is modeled based on a realistic three-dimensional approach, in other words, the geometry of the embossment is represented in detail in order to reproduce the actual mechanical interaction between the materials and the embossments. The interface between steel and concrete was simulated face-to-face using contact elements, which is the usual approach in ANSYS. One surface is defined as “target”, in this case the concrete, and the other surface is defined as “contact”, in this case the steel. For the first surfaces the finite element TARGE170 [18] is adopted, which describes the boundary of a deformable body. For the second surfaces (“contact”) the CONTA174 elements are associated. Contact occurs when the CONTA174 contact elements penetrate one of the target elements defined by TARGE170. The normal pressure equals zero if any kind of separation occurs.

In this work, the chemical bond between the sheet metal and the concrete is not modeled, in other words, the effect is neglected, since the contribution of the initial bond to the ultimate strength is negligible, according to experimental results for galvanized steel [12]. In addition, for tests of composite slabs, some procedures provide for lubrication of the slabs before concreting, in an attempt to make a more conservative estimate of the longitudinal shear strength as a contribution of the embossments only (*Avis* technique) [22].

The friction model adopted between the surfaces after they come into contact is based on Coulomb's law. The coefficient of friction is defined as isotropic and static (due to the low speed of load application in the composite slab test), in other words, independent of the direction of sliding tendency during contact, with Coulomb's law behaving in the same way. The value used for the friction between galvanized sheets and concrete is 0.2 [12].

### 2.4 Loading and support of the nonlinear analysis

The loading applied to the finite element method models was controlled through prescribed displacement. The loading is applied prescribing displacement at a line of nodes at the concrete surface. The ultimate loads of the simulations are thus measured at the reaction support (total forces at the support at each step). The four-point bending test is simulated in ANSYS by means of incremental static analysis (monotonic) in a nonlinear regime. The Newton-Raphson algorithm [23] was used.

The displacement was applied to the fourth part of the shear span, as shown in Figure 9. The support is defined by restricting the displacement of a line of nodes at the bottom of the profiled sheeting and was applied 89 millimetres from the beginning of the span (Figure 9). In this case, 89 millimetres is the length of the small module possible, as will be explained in the next sections.

### 2.5 Symmetry

Three conditions of symmetry were used, as shown in Figure 9, where there are two planes of transverse symmetry and one plane of longitudinal symmetry present on the side of the smallest model necessary for geometric modeling. Thus, it was possible to mirror the module in relation to the center of the slab and repeat one on each side, equalling a prototype with three ribs along the width. Because of the symmetrical finite element strategy adopted, an assumption is made that the ultimate loads computed as the total forces at the support must be multiplied by three, considering the presence of three ribs when adopting symmetry.

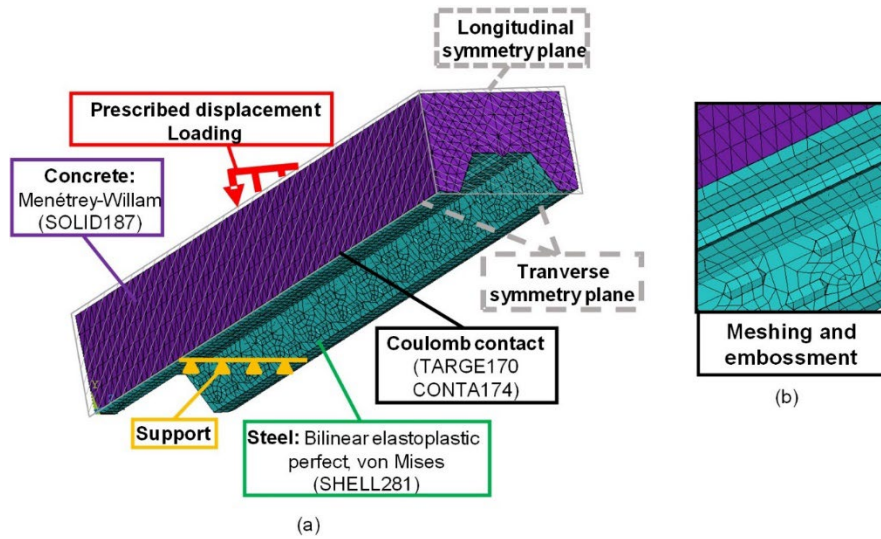


Figure 9. Finite element computational model description with planes of symmetry.

### 2.6 Embossments meshing

The mesh description was performed throughout the model, as shown in Figure 9b, and according to each of its elements, always seeking the most regular shape to represent it, in order to avoid highly distorted finite elements. The average global mesh size inputted in software was 13 millimetres and this value was reached after a mesh quality study carried out in the context of a Master Thesis supported this article [24]. Measurements used for the Polydeck 59s formwork were obtained through on-site measurements. It is also possible to observe that the numerical model represents the real geometry of the steel formwork with a good approximation (see Figure 10). It is important to bear in mind that the modelling of the embossments is an approximated geometry modelling strategy, disregarding the small radiuses involved in the process of manufacturing the embossments over the steel sheet. In other words, the “real curved” geometry of the embossment is approximated by median planes with a good fit. Of course, the geometry of the embossments is approximated due to limitations of the finite element analysis. This limitation is related to possible convergence problems of the results common in material and geometrical nonlinear analyses. In the steel sheet investigated there are two rows of embossments, while in the original steel sheet investigated in the work of Soltanalipour et al. [12] there was only one row of embossments, thus requiring modifying the geometry to add more embossments. Figure 10b shows the adopted simplified geometry for the embossments. Width and height are presented in Figure 10b. The total depth of the embossment was measured and modelled as nearly 4 mm, with small variations according to the simulated nominal thickness (0.80, 0.95 and 1.25 mm), since the shell elements are modelled centered in the mid-layer.

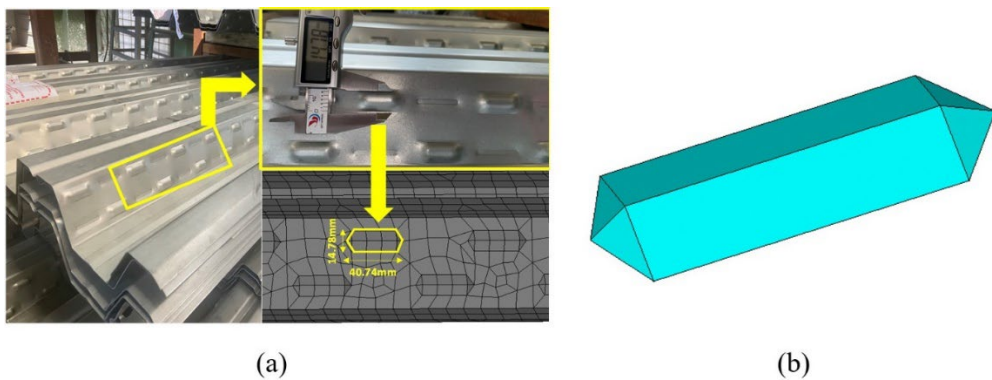


Figure 10. (a) Polydeck 59s metal formwork with on-site measurements and numerical model with representation of the (b) simplified geometry of the embossment.

### 2.7 Smallest repeatable module

An 89 millimetres module (see Figure 11) was developed and repeated as many times as necessary to reach the span value for each prototype (Figure 11d). Of course, the desired span lengths were multiple of the module length. Two embossments are represented in each module, as shown in the Figure 11c. Except from the embossments, the module is symmetrical, in other words, it has the same geometry when mirrored with respect to the central axis. However, the embossments occupy alternated positions in the longitudinal direction when considering neighbouring faces. This was also included in the finite element model developed in this work. This is made to increase the interlocking effect against longitudinal failure. A plane open crack higher than the steel profile is considered to represent the experimental crack inducers ruled by Eurocode and usually used in real tests (Figure 11e). At this plane of the crack inducer, the elements do not share the same nodes, thus creating a discontinuity in the finite element mesh, avoiding the transmission of tensile stresses throughout these sections, as this is the intended effect from crack inducer, clearly defining a shear span. The crack inducer is located 5 millimetres below the top face of the composite slab and has a width dimension equivalent to that of the repeatable module (full width). Contact surfaces between the two faces of the crack were not employed, due to the fact that they are supposed to keep departing since the beginning of the loading. The mesh was not refined at the tip of the crack, since the stress field ahead of the crack tip for the specific purpose of the herein presented simulation (to evaluate the longitudinal shear strength) is not considered relevant. From Figure 11c one may note that the embossments are very near to the limits of the module, approaching the end of the module length, but not touching it. This was made on purpose, in order to avoid highly distorted elements generated by the automatic mesh algorithm at these highly irregular regions. In this case, putting the embossments end far from 3 up to 4 millimetres from the module end was sufficient to not generate poor elements. This was not a problem in the original work of [12], since their embossment was only one, and it was positioned at the center of the module.

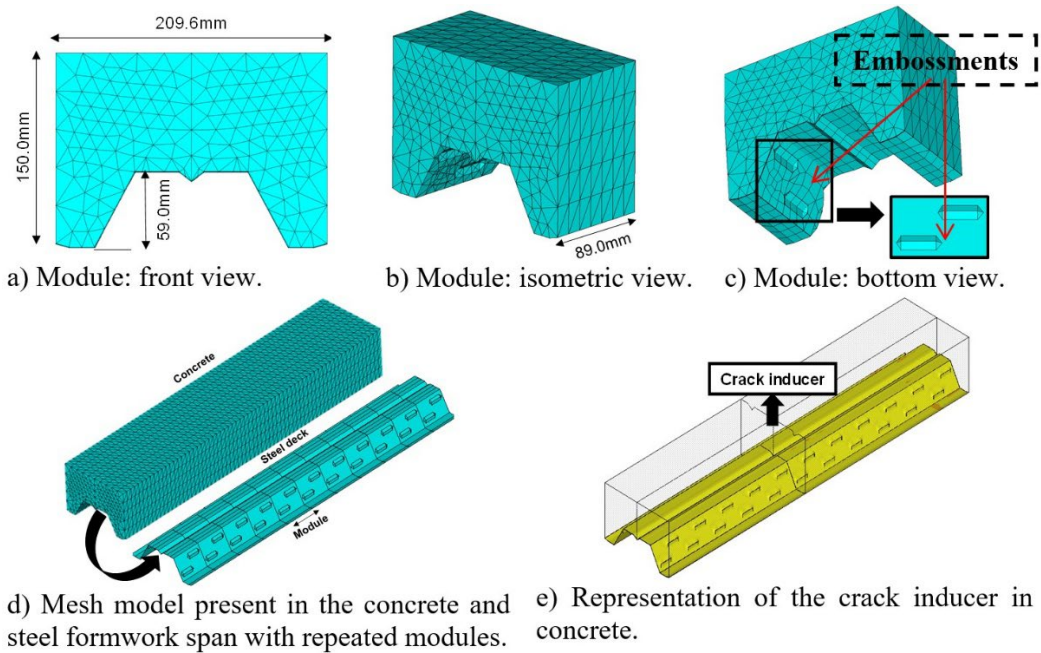


Figure 11. Geometry of the finite element model developed in the present work.

### 2.8 Characteristics of the simulated structural models

Having performed all the definitions with the properties of each material, constitutive models, finite elements, contact between materials, mesh and symmetry in this article, a minimum value was chosen in relation to the shear span, which in this case is 1.40 meters, this span was chosen because it is one of the smallest spans seen in a project. The span of 2.80 meters is often used in typical designs of floors with composite slabs. Thus, six simulations were performed with prototype heights of 15 centimetres, and shear spans ( $L_s = L/4$ ) varying between 350, 450, 625 and 700 millimetres, and thicknesses between 0.8, 0.95 and 1.25 millimetres as presented in Table 3. Each prototype was identified with the name of structural model (SM) with its respective number that refers to the order in which each simulation was run, ranked from I to VI.

**Table 3.** Characteristics of the simulated structural models.

Identifier	t (mm)	L (mm)	L <sub>s</sub> (mm)
SM-I	0.80	1800	450
SM-II	0.80	2800	700
SM-III	0.95	1800	450
SM-IV	0.95	2500	625
SM-V	1.25	1800	450
SM-VI	1.25	1400	350

### 3 RESULTS AND DISCUSSION OF THE FINITE ELEMENT ANALYSES

At first, the results of the finite element nonlinear analyses for the six structural models are presented in Figures 12 and 13, showing results in terms of total vector displacements (labels (a), (c) and (e)) and stresses in longitudinal direction Z for the steel sheet only (labels (b), (d) and (f)). The results are shown for the ultimate load step (that is, the step for which the total forces at the support begin to decrease – ultimate load capacity of the simulation). In Figures 12a, 12c, 12e and Figures 13a, 13c, 13e one can see the concrete part of the composite slab joined at the top only by a row of elements, the crack fully opened, and the detachment of the steel sheet from the concrete part in the constant moment region (also shown in Figure 14). Figure 15 represents the deflection and slip parameters that can be analysed in this failure mode. Table 4 shows the value of each of these points in each of the simulated structural models at the ultimate load step. In Figures 12b, 12d, 12f and Figures 13b, 13d, 13f one can see the bottom flanges of the rib tensioned and the top flanges of the rib compressed. In the constant moment region there is effect of isolated bending of the sheet and the concrete part, while in the shear span this effect is less experienced.

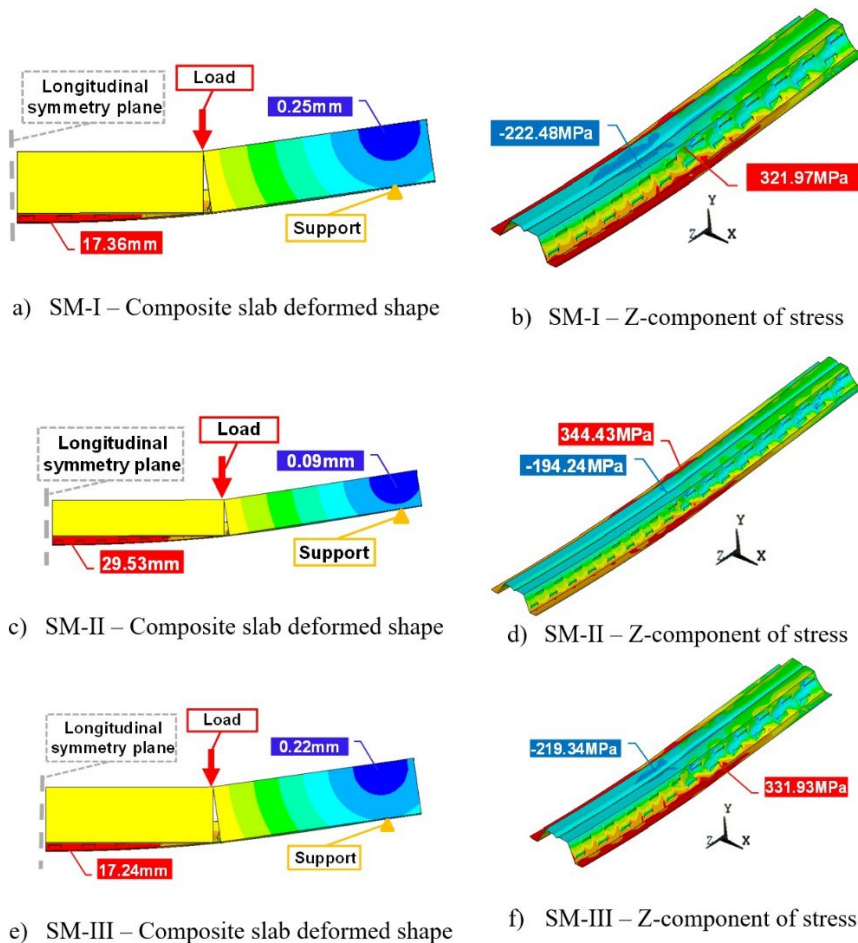


**Figure 12.** Results for the investigated structural models: (a), (c) and (e) total vector displacements; (b), (d) and (f) stresses longitudinal direction (Z-component).

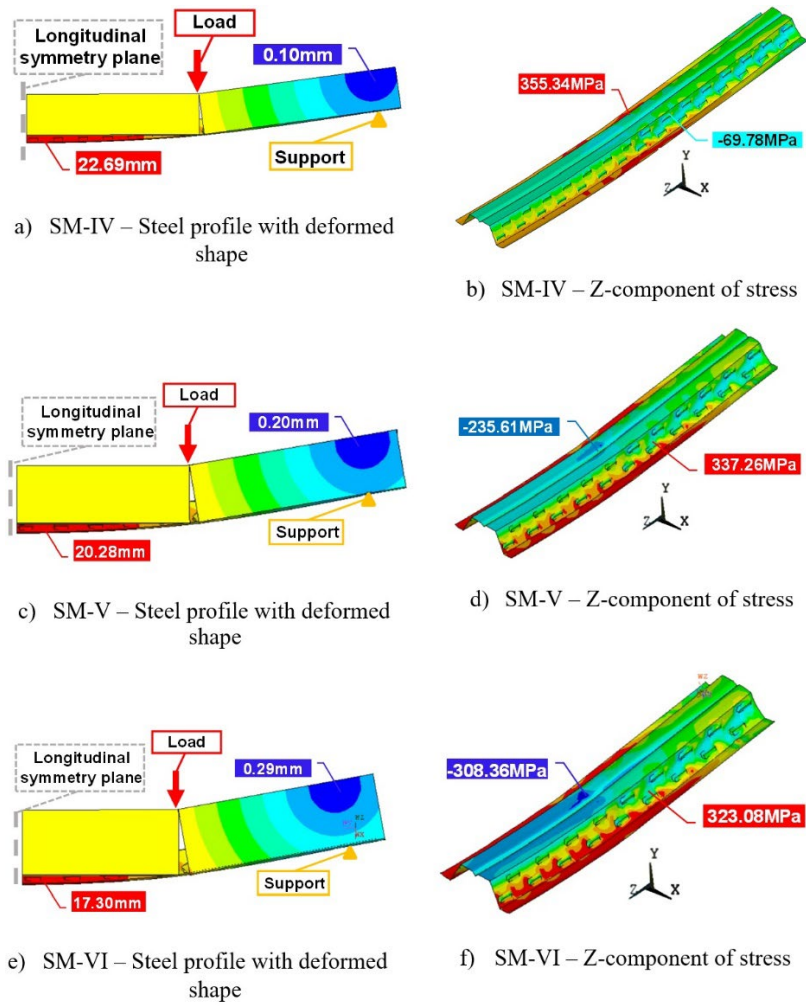


**Figure 13.** Results for the investigated structural models: (a), (c) and (e) total vector displacements; (b), (d) and (f) stresses longitudinal direction (Z-component).

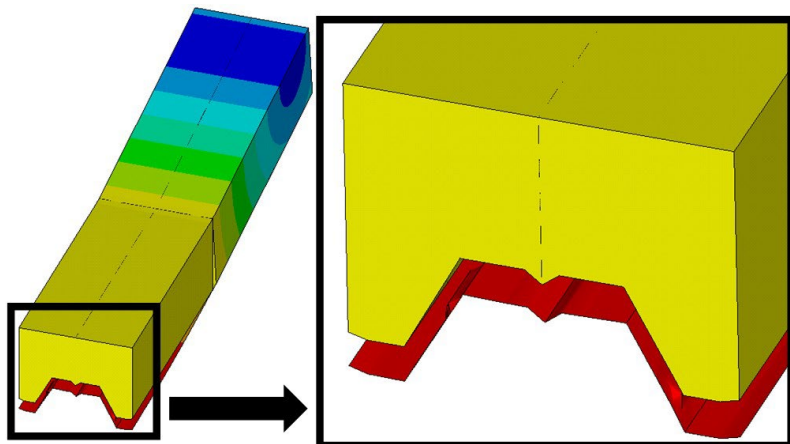


**Figure 14.** Vertical detachment between the steel formwork and the concrete found in the finite element simulation.

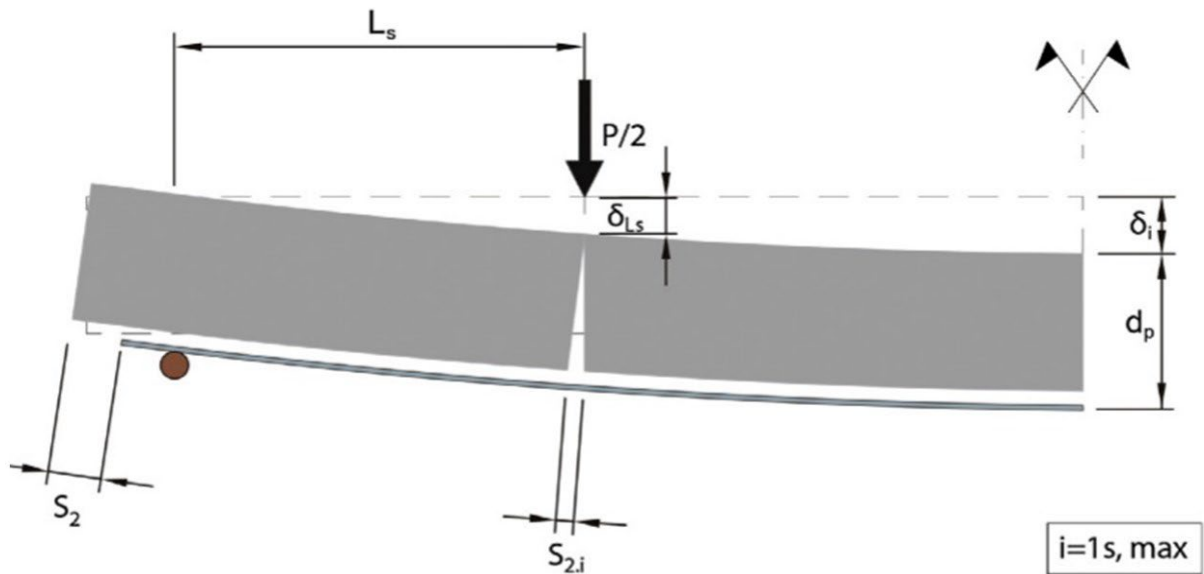


Figure 15. Indicators for locating the deflection and slip parameters [25].

Table 4. Deflection and slip values determined from the numerical analyses (the parameters are represented in Figure 15).

Identifier	$L_s$ (mm)	$d_{LS}$ (mm)	$d_i$ (mm)	$S_2$ (mm)	$S_{2,i}$ (mm)
SM-I	450	12.72	12.94	2.89	4.06
SM-II	700	21.80	22.22	2.89	4.28
SM-III	450	12.72	12.96	3.70	4.03
SM-IV	625	16.88	17.28	2.41	3.74
SM-V	450	15.14	15.49	4.65	4.76
SM-VI	356	12.87	13.18	3.58	5.12

The horizontal slip ( $S_2$ , refer to Figure 15) between the steel formwork and the concrete found in the finite element simulation can be seen in Figure 16. It is important to note that the factors that influence this sliding are the chemical bond between the concrete and the steel, the mechanical bond that occurs through the dents, and the friction between the formwork and the concrete. In this work, both mechanical bonding and friction are present, which is made present by using the value of the coefficient of friction of 0.2 [12]. One may see that the failure generally occurs for a slip of about 3 to 4 millimetres, which is consistent with values found in literature [26].

Figure 17 shows the results of the vertical displacements at mid-span in relation to loads “P” (refer to Figure 15). In this graph it is possible to identify the peak load for each of the simulations. It is worth noting that in this numerical simulation model it is not possible to obtain the results of pre-cracking of the concrete, because cracking inducers were used, in other words, since the beginning of loading there was already cracked concrete.

Together with the nonlinear curve in Figure 17, a black straight line represents the linear-elastic stiffness (force versus displacement) considering the cracked moment of inertia computed, where “C.S.” stands for cracked section moment of inertia. For the very initial steps of loads, the red curves are relatively consistent with the linear stiffness, and after a few steps they differ. This can be caused because of the nonlinear behavior and also because of the presence of the crack at almost full height in the finite element analysis. However, it is already known from other works that the computations of displacements in composite slab systems using the linear-elastic theory with cracked section moment of inertia are nonconservative, and Costa et al. [27] presented a methodology to improve the computation of displacements with more advanced formulations. Moreover, it was observed that first yielding of materials occurs after major change of slope of the load versus displacement relation.

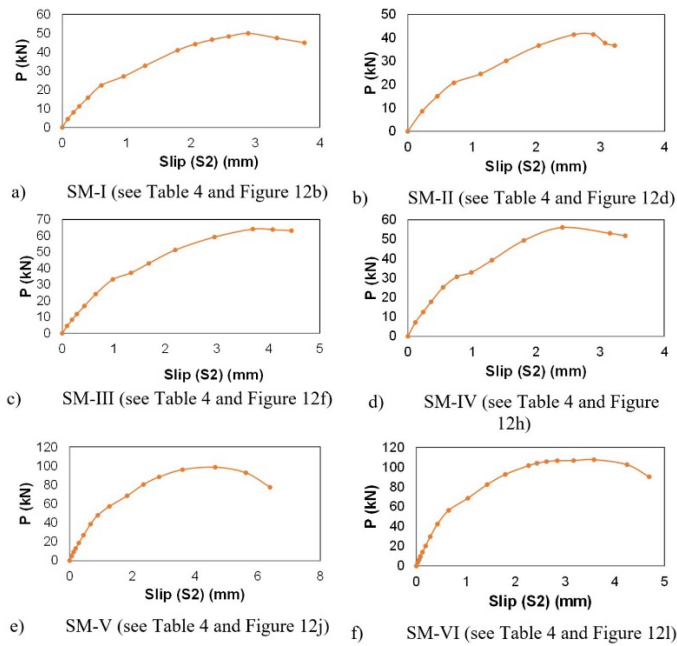


**Figure 16.** Numerical simulations of the structural models: force versus slip ( $S_2$ ) curves

After performing the simulations, the ultimate load results ( $P_{u,FEM}$ ) were obtained for the carried out analyses as presented in Table 5. Thus, it was possible to use these load results and obtain the linear regression graph to obtain the coefficients  $m$  and  $k$ , as presented in Figure 18. Thus, it is concluded that the trend line presents a good performance by presenting a linear correlation value ( $R$ ) equal to 0.97, with the relationship between the Y axis explained in 94% by the X axis ( $R^2=0.94$ ). A standard deviation of 0.18 was also found, which is for ultimate strength capacity estimations in structural analysis field a good value. A comparison with the mean values (without safety factor) obtained with Equation 1 employing the estimated m-k coefficients is also presented.

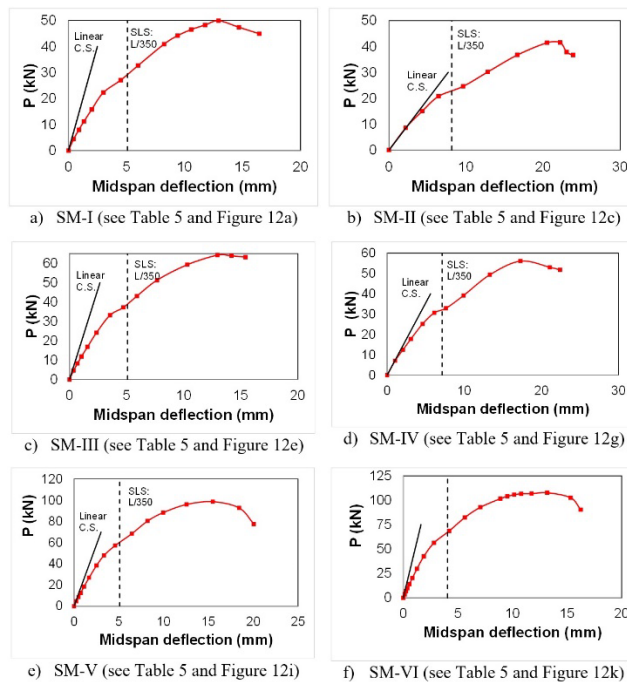


**Figure 17.** Numerical simulations of the structural models: force  $P$  (refer to Figure 15) versus midspan deflection curves.

**Table 5.** Ultimate load results found in the numerical simulations.

Identifier	t (mm)	L (mm)	L <sub>s</sub> (mm)	P <sub>u,FEM</sub> (kN)	V <sub>Lu,FEM</sub> = 0.5P <sub>u,FEM</sub> (kN)	V <sub>L,k</sub> (kN) Equation 1	Diff.
SM-I	0.80	1800	450	49.91	24.96	29.36	15.0%
SM-II	0.80	2800	700	41.52	20.76	19.54	6.0%
SM-III	0.95	1800	450	64.20	32.10	34.52	7.0%
SM-IV	0.95	2500	625	56.09	28.05	25.56	10.0%
SM-V	1.25	1800	450	98.76	49.38	44.86	10.0%
SM-VI	1.25	1400	350	107.77	53.89	55.28	3.0%

It is also possible to verify that the results found for the values of the coefficients *m* and *k* in this finite element simulation are within the standards of the results presented in the research works presented in Table 6. In Figure 19, it is possible to observe more clearly the results obtained in this study when compared with the results found in the literature.

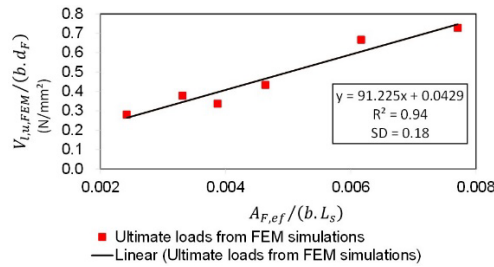


**Figure 18.** Linear regression of the results obtained in the numerical simulations.

**Table 6.** Some values of *m* and *k* found in the literature.

Module	Height (mm)	Width (mm)	Embossment Type	<i>m</i> (N/mm <sup>2</sup> )	<i>k</i> (N/mm <sup>2</sup> )	Author
	46	900		107.53	0.040	Wright et al. [28]
	76	914		84.67	0.022	Chen [29]
	55	820		87.96	0.032	Marimuthu et al. [30]
	60	820		98.32	0.080	O Feliz [31]
	52	830		81.95	0.046	Hedaoo et al. [32]
	61	820		95.69	0.022	Soltanalipour et al. [33]

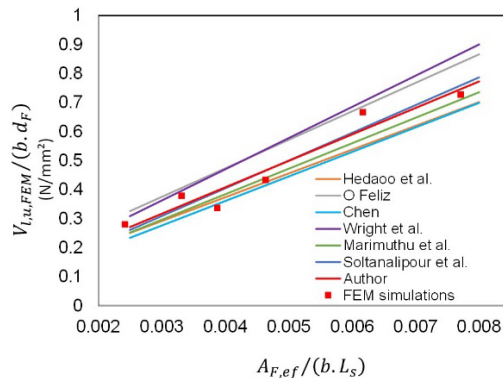


**Figure 19.** Linear regression of coefficients *m-k* in literature and results obtained in the developed numerical simulations.

### 3.1 Influence of the presence or absence of explicitly modelled embossments

In order to show the influence of embossments and demonstrate the capabilities of explicitly modelling its geometry in the FE model in the present methodology, a few more analyses are discussed in the present section. Of course, the total longitudinal shear strength can be separated into the contribution of the mechanical contact of the concrete parts with the steel embossments and the friction between the steel parts and the concrete. Below in Figure 20 it is represented the load versus midspan deflection curve of a selected analysis, considering a simply supported span of 1.4 m, total slab height of 110 mm, nominal steel sheet thickness of 1.25 mm and average concrete strength of 41 MPa (this analysis was selected because it contain less elements and can be simulated more quickly). In this curve, one can identify four different load levels: (1) elastic range; (2) inelastic range; (3) ultimate load peak and (4) post-peak load. Then, in Figure 21 it is represented the contour stress plots of the longitudinal contact stresses in the bottom face of the concrete part in the constant shear span ( $L_s$ ), showing only the concrete part (omitting the steel sheet thickness for illustration purposes). Therefore, one can see the cavities created by the steel embossments in the concrete in this figure. The maximum normal contact stress (of compression) is the following in the four levels, respectively: -14.06 MPa (elastic), -30.01 MPa (inelastic), -39.16 MPa (load peak), and -34.6 MPa (post-peak), highlighting the working contact stresses concentrated in the concrete cavities throughout the whole analysis (thus illustrating the mechanical contact provided by the embossments), and its decrease after the load peak. The remaining concrete parts remain with much lower compressive stresses.

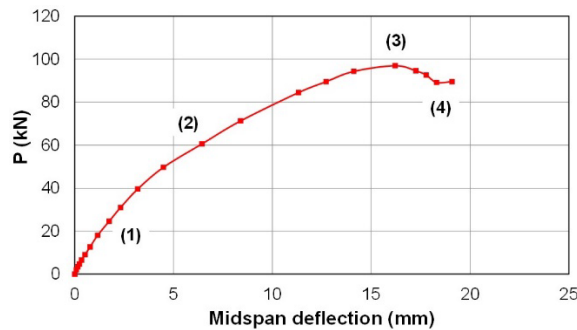


**Figure 20.** Load versus midspan deflection of a simulation assuming: total slab height of 110 mm; nominal steel sheet thickness of 1.25 mm; concrete  $f_{cm}$  of 41 MPa; simply-supported span of 1.4 m; friction coefficient of 0.2.

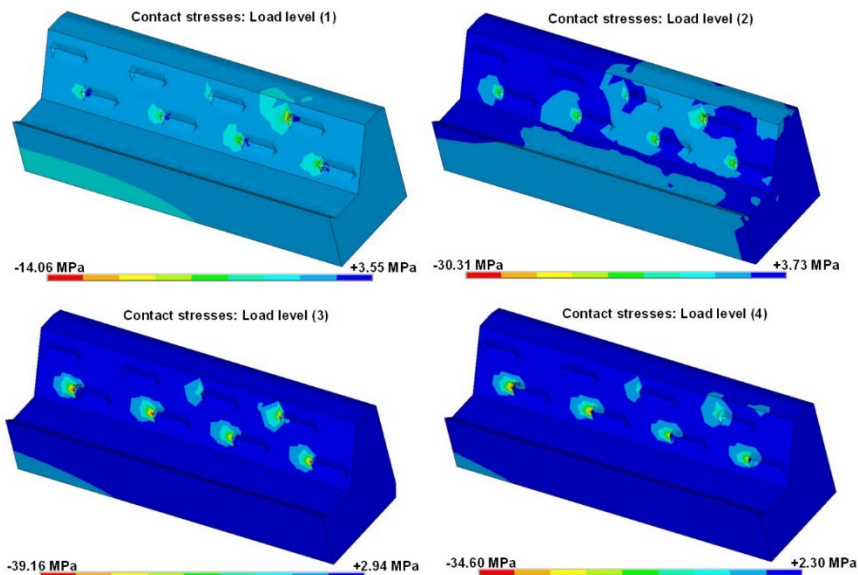


**Figure 21.** Various contact stress load levels (longitudinal direction) in the concrete elements in the bottom face (half rib) showing stress concentration in the cavities created by steel sheet embossments: load levels (1) to (4) (refer to Figure 20).

Only the shear span is illustrated, because the cavities created by embossments in the concrete part in the constant moment region do not present the same behavior, with absence of contact stresses due to the mechanical contact between steel and the concrete in this region. This is due to the debonding effect, which for the present simulations occurs since very early stages of loading for the constant moment region. Of course, in order to present composite action, it is necessary to exist vertical shear, which in turn will create shear flow between both parts through the shear devices (herein represented by embossments). In other works, as discussed in the introduction of the present paper, this effect was simulated only by friction, by artificially increasing the friction coefficient to calibrate the simulation. Thus, in order to compare with the present methodology, a model without embossments for which the longitudinal shear is transferred only through friction was created (see Figure 22 for a bottom view of this model). It considered a total slab height of 150 mm, a simply supported span of 1.4 m, an average concrete strength of 41 MPa and friction coefficient varying from 0.2 to 0.9 (highest value used in Soltanalipour et al. [12]). Then, four more analysis were carried out: (1) explicitly modelling embossments and using a friction coefficient of 0.2; (2) without considering embossments geometry and using a friction coefficient of 0.2; (3) explicitly modelling embossments and using a friction coefficient of 0.9, and (4) without considering embossments geometry and using a friction coefficient of 0.9. The results are shown in Figure 23. One can see that without considering embossments geometry and a using friction coefficient of 0.9 the maximum ultimate load was of 54.99 kN, while considering the same friction coefficient but explicitly modelling embossments was obtained a value of 191.50 kN, an increase of nearly three-fold and half. By adopting a friction coefficient of 0.2, the increase is in the order of two-fold and half. Thus, it was observed that the influence of directly modelling the embossments is greater the greater the friction coefficient, and from these analysis the contribution of each one for the ultimate load can be partially separated.

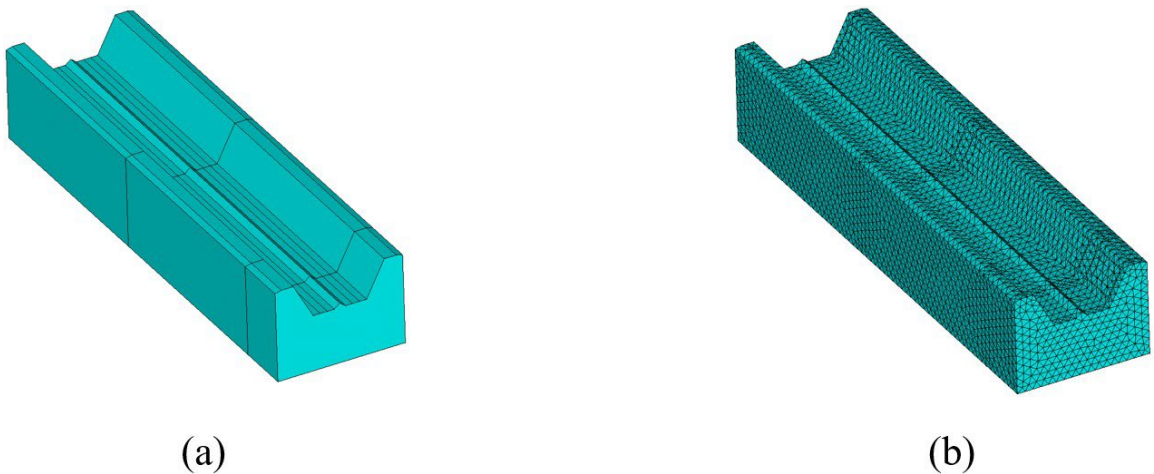


**Figure 22.** A view of the model without explicitly considering embossments geometry: (a) volumes used in discretization, with only three separations marking the midspan symmetry plane, the position to apply loads and the support; (b) finite element mesh of the model without embossments.

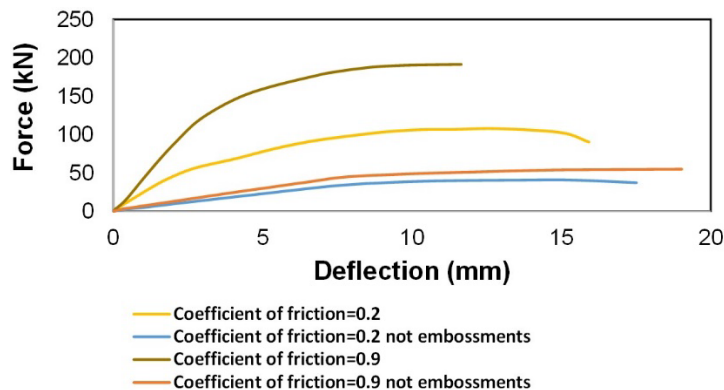


**Figure 23.** Four simulations of a preliminary study of the influence of embossments versus friction coefficient.

## 4 CONCLUSIONS

It can be concluded that the finite element model developed in this work enabled a good representation of the parameters involved, despite having limitations when compared to experimental research it is still an excellent tool to carry out studies on composite slabs with steel deck. With this in mind, the following conclusions can be extracted from the present study:

- With the use of symmetries and repeatable modules along the span, the computational cost of these numerical studies is considerably reduced, allowing the variation of the steel formwork geometry to represent almost any type of irregularity. In addition, the use of adequate meshes allows the model to have better conditions to converge in its results;
- It is also important to note that before deeper conclusions can be extracted from the results of the numerical analyses, the finite element models need to be calibrated with experimental results, although the present methodology was adapted and modified from a study where it was calibrated against other steel deck, giving to it more reliability to be applied to other geometries, a task that was made in the present study. In this sense, a very good regression analysis was obtained, achieving  $R^2$  equal to 0.94 and a standard deviation of 0.18.

On the other hand, from the comparisons of experimental results from literature with the nonlinear results with the present work using the adapted and proposed methodology, some remarks can be made regarding the limitations of the finite element analysis, for example:

- During experimental tests of composite slabs, two load drops are generally observed. The first load drop is usually associated with the loss of adherence between the steel sheet and the concrete between the two loads (in the constant moment region). The second load drop is usually associated with crack growth induced by crack inducers in the sections of load application from the crack inducer height up to the crack control reinforcement (in experimental tests the crack grows almost up to the top of the concrete section). Of course, in order to overcome this limitation (because no fracture mechanics model is adopted in the present methodology), the total crack height is included since the beginning of the analysis, thus considering a lower bending stiffness for the complete analysis, which justifies the relatively higher displacements in the finite element analysis in the beginning of the simulation when comparing with computations using the linear-elastic assumptions (even using the cracked moment of inertia), as was shown in Figure 17;
- During the analysis, the position of the initial crack height in the finite element analysis, representing the final stage of the crack growth during tests was noted to highly influence the ultimate loads. The herein presented results were computed considering the crack height at the load lines leaving just a single row of elements connected at the top;
- The methodology herein presented and adapted from a previous work [11] do not consider any chemical adherence between materials, although as discussed this is consistent with experimental tests using oil (French *Avis* technique), which tries to eliminate this contribution in the analysis. Besides that, the supports are simulated in the finite element analysis as “concentrated” lines, that is, a line of nodes which resists the vertical loads. This is a simplification, since at experimental tests the support occurs along a length of 100 millimetres as ruled by Eurocode as the standard support length. One may note that the effect of friction at supports, which contributes to increase the total longitudinal shear strength depends on the area of contact, and obviously in this case a “concentrated” line of restricted nodes to vertical displacements limits the area of contact, thus slightly modifying the effect of friction at supports. Another inconvenient not commented and discussed in the original work of [11] is that during the nonlinear analysis, some nodes along this “concentrated” lines present negative reactions (that is, the steel sheet trying to up lift at some nodes), although limited to negligible values. In the present work, only the positive values of reactions at the supports were used (summed) to compute the ultimate loads and construct the graphs shown in Figures 16 and 17. In order to avoid this effect, a nonlinear support must be included, but this can be highly cost in terms of computational time and also increase the difficulty to achieve convergence.

Future research works may include the variation of more structural parameters and their corresponding influence on the design shear strength of composite slabs. In this context, the finite element analysis can be an excellent tool to study and optimize the shape of embossments to achieve higher longitudinal shear strengths. In this sense, this work is a first step in this direction.

## ACKNOWLEDGEMENTS

Finally, in gratitude, this work was made possible by the support of Coordenação de Aperfeiçoamento de Pessoal de Nível Superior (CAPES) and ArcelorMittal Brasil.

## REFERENCES

- [1] Associação Brasileira de Normas Técnicas, *Projeto de Estruturas de Aço e de Estruturas Mistas de Aço e Concreto de Edifícios*, ABNT NBR 8800, 2008.
- [2] C. Santos and M. Malite, “Análise numérica de lajes mistas de aço e concreto,” in *8º Congr. Latin.-Amer. Const. Met. Construmetal 2019*, 2019, pp. 1–28.
- [3] Comitê Europeu de Normalização, *Projeto de Estruturas Mista de Aço-Betão - Parte 1-1: Regras Gerais e Regras para Edifícios*, EN 1994-1-1, 2011.
- [4] C. S. Young and W. S. Easterling, “Strength of composite slabs,” in *Int. Spec. Conf. Cold-Form. Steel Struct.*, 1990, pp. 65–80, [http://dx.doi.org/10.1061/\(asce\)0733-9445\(1992\)118:9\(2370\)](http://dx.doi.org/10.1061/(asce)0733-9445(1992)118:9(2370)).
- [5] L. D. Luttrell and S. Prasanna, “Strength formulations for composite slabs,” in *Proc. 7th Int. Spec. Conf. Cold-Form. Steel Struct.*, 1984, pp. 307–324.
- [6] I. Shobaki, “The behaviour of profiled steel sheet/concrete composite slabs,” Ph.D. dissertation, Univ. Salford, Salford, United Kingdom, 2000.
- [7] B. J. Daniels and M. Crisinef, “Composite slabs behavior and strength analys. Part II: comparisions with test resultas and parametric analysis,” *Eng. Struct.*, vol. 119, no. 1, pp. 36–49, Jan. 1993.
- [8] S. Chen and X. Shi, “Shear bond mechanism of composite slabs - a universal FE approach,” *J. Construct. Steel Res.*, vol. 67, no. 10, pp. 1475–1484, Oct. 2011, <http://dx.doi.org/10.1016/j.jcsr.2011.03.021>.
- [9] A. Gholamhoseini, R. I. Gilbert, M. A. Bradford, and Z. T. Chang, “Longitudinal shear stress and bond-slip relationships in composite concrete slabs,” *Eng. Struct.*, vol. 69, pp. 37–48, Jun. 2014, <http://dx.doi.org/10.1016/j.engstruct.2014.03.008>.
- [10] A. R. Silva and P. B. Silva, “Nonlinear numerical analysis of composite slabs with steel decking,” *Rev. IBRACON Estrut. Mater.*, vol. 12, no. 5, pp. 972–997, Sept./Oct. 2019, <http://dx.doi.org/10.1590/s1983-41952019000500002>.
- [11] A. Gholamhoseini, “Experimental and finite element study of ultimate strength of continuous composite concrete slabs with steel decking,” *Int. J. Adv. Struct. Eng.*, vol. 10, no. 1, pp. 85–97, Mar. 2018, <http://dx.doi.org/10.1007/s40091-018-0183-3>.
- [12] M. Soltanalipour, M. Ferrer, and F. Marimon, “Experimental and numerical study of the ductility of open-rib and reentrant composite slabs,” *Eng. Struct.*, vol. 256, pp. 113984, Apr. 2022, <http://dx.doi.org/10.1016/j.engstruct.2022.113984>.
- [13] Associação Brasileira de Normas Técnicas, *Projeto de Estruturas de Concreto -Procedimento*, ABNT NBR 6118, 2014. Accessed: Oct. 11, 2023. [Online]. Available: <https://www.abntcatalogo.com.br/pnm.aspx?Q=WDg4WU1kOGI0NWpWUVJnLzF5VEV3TVRWN2tSURpSGI4Y0I1VkNwckIyST0=>
- [14] Associação Brasileira de Normas Técnicas, *Dimensionamento de Estruturas de Aço Constituídas por Perfis Formados a Frio*, ABNT NBR 14762, 2010.
- [15] Associação Brasileira de Normas Técnicas, *Ações para o Cálculo de Estruturas de Edificações*, ABNT NBR 6120, 2019.
- [16] ArcelorMittal Perfilor, *Catálogo Técnico Polydeck 59S*, 12th ed. São Paulo: ArcelorMittal Perfilor, 2016.
- [17] ASTM International, *Standard Test Methods for Tension Testing of Metallic Materials 1*, ASTM E8/E8M, 2010, <http://dx.doi.org/10.1520/E0008>.
- [18] ANSYS Element Reference, *ANSYS Mechanical APDL Element Reference*. Canonsburg, PA. EUA: Ansys, 2021.
- [19] P. Menétrey, *Numerical Analysis of Punching Failure in Reinforced Concrete Structures*. Lausanne, Switzerland: EPFL, 1994.
- [20] K. J. Willam and E. P. Warnke, “Constitutive model for the triaxial behaviour of concrete,” *Proc. Int. Assoc. Bridg. Structl. Eng.*, vol. 19, pp. 1–30, 1975.
- [21] P. C. S. Silva, “Resistência à tração de diferentes tipos de ancoragens embutidas em elementos de concreto armado,” Master thesis, Prog. Pós-Grad. Estrut. Constr. Civil, Univ. Brasília, Brasília, Brazil, 2018.
- [22] European Convention for Constructional Steelwork, *Longitudinal Shear Resistance of Composite Slabs: Evaluation of Existing Tests*, ECCS TC 7, 1998.
- [23] L. E. Vaz, *Método dos Elementos Finitos em Análise de Estruturas*. Rio de Janeiro: Elsevier, 2011.
- [24] J. H. L. P. Mello, “Avaliação da resistência de lajes mistas com fôrma de aço incorporada por modelagem em elementos finitos considerando a geometria das mossas,” Dissertation, Univ. Brasília, Brasília, Brazil, 2023.
- [25] J. D. Ríos, H. Cifuentes, A. Martínez-De La Concha, and F. Medina-Reguera, “Numerical modelling of the shear-bond behaviour of composite slabs in four and six-point bending tests,” *Eng. Struct.*, vol. 133, pp. 91–104, Feb. 2017, <http://dx.doi.org/10.1016/j.engstruct.2016.12.025>.

- [26] C. B. Ferraz, “Análise do comportamento e da resistência do sistema de lajes mistas,” Master thesis, Prog. Pós-Grad. Eng. Estrut., Esc. Eng., Univ. Fed. Minas Gerais, Belo Horizonte, Brazil, 1999.
- [27] R. S. Costa, A. C. C. Lavall, R. G. L. Silva, H. F. Viana, F. C. Rodrigues, and E. L. Andrade, “New equations to establish the effective moment of inertia of composite slabs with profiled steel sheeting for deflection calculation,” *J. Build. Eng.*, vol. 37, pp. 102135, Dec. 2021, <http://dx.doi.org/10.1016/j.jobe.2020.102135>.
- [28] H. D. Wright, H. R. Evans, and P. W. Harding, “The use of profiled steel sheeting in floor construction,” *J. Construct. Steel Res.*, vol. 7, no. 4, pp. 279–295, 1987, [http://dx.doi.org/10.1016/0143-974X\(87\)90003-4](http://dx.doi.org/10.1016/0143-974X(87)90003-4).
- [29] S. Chen, “Load carrying capacity of composite slabs with various end constraints,” *J. Construct. Steel Res.*, vol. 59, no. 3, pp. 385–403, Mar. 2003, [http://dx.doi.org/10.1016/S0143-974X\(02\)00034-2](http://dx.doi.org/10.1016/S0143-974X(02)00034-2).
- [30] V. Marimuthu, S. Seetharaman, S. A. Jayachandran, A. Chellappan, T. K. Bandyopadhyay, and D. Dutta, “Experimental studies on composite deck slabs to determine the shear-bond characteristic (m - k) values of the embossed profiled sheet,” *J. Construct. Steel Res.*, vol. 63, no. 6, pp. 791–803, Jun. 2007, <http://dx.doi.org/10.1016/j.jcsr.2006.07.009>.
- [31] O Feliz, *Laje Mista - Perfil H60*. Braga, Portugal: O Feliz, 2011.
- [32] N. A. Hedao, L. M. Gupta, and G. N. Ronghe, “Design of composite slabs with profiled steel decking: a comparison between experimental and analytical studies,” *Int. J. Adv. Struct. Eng.*, vol. 4, no. 1, pp. 1–15, Sept. 2012, <http://dx.doi.org/10.1186/2008-6695-3-1>.
- [33] M. Soltanalipour et al., “Shear transfer behavior in composite slabs under 4-point standard and uniform-load tests,” *J. Construct. Steel Res.*, vol. 164, pp. 105774, Jan. 2020, <http://dx.doi.org/10.1016/j.jcsr.2019.105774>.

---

**Author contributions:** JHLPM: investigation, data curation, formal analysis, methodology, writing (original draft), software; DQP: tensile strength test, review and editing; MPM: review and editing; HSC: conceptualization, review and editing; RML: funding acquisition, supervision, project administration, conceptualization, writing, review and editing; LACMV: tensile strength test, review and editing; JLVB: tensile strength test, review and editing; JGSS: review and editing; GSA: investigation, conceptualization; supervision, methodology, writing, review and editing, software. All authors have read and agreed to the published version of the manuscript.

**Editors:** Mauro Real, Guilherme Aris Parsekian.